JOURNAL OF MATERIALS SCIENCE **40** (2005) 591–595

Two-dimensional SnS nanosheets fabricated by a novel hydrothermal method

HONGLIANG ZHU*
Center of Materials Engineering, Zhejiang University of Sciences, Hangzhou 310033, People's Republic of China
State Key Lab of Silicon Materials, Zhejiang University, Hangzhou 310027, People's Republic of China
E-mail: webmaster@51yq.com

DEREN YANG, YUJIE JI, HUI ZHANG
State Key Lab of Silicon Materials, Zhejiang University, Hangzhou 310027, People's Republic of China

XIAOFEI SHEN
Center of Materials Engineering, Zhejiang University of Sciences, Hangzhou 310033, People's Republic of China

Two-dimensional (2D) Tin (II) sulfide (SnS) nanosheets were successfully synthesized by a novel thioglycolic acid (TGA) assisted hydrothermal method. X-ray diffraction characterization reveals that the product is well-crystallized SnS with orthorhombic structure. Transmission electron microscopy observation shows that the SnS crystals display 2D sheet-like nanomorphology. Further structure characterization by selected area electron diffraction identifies that the SnS nanosheets are single crystalline in nature. Furthermore, the mechanism and critical factors for the TGA-assisted hydrothermal synthesis of the SnS nanosheets have been preliminarily discussed.

1. Introduction

Semiconductor nanostructures have been attracting worldwide attention due to their exceptional eletrical, optical and magnetic properties, and their potential applications in nanoscale eletronics, photonics and functional materials as well [1–3]. Among them, tin (II) sulphide (SnS) has sparked intensive interest for its semiconducting and optical properties. SnS, as one of important IV–VI group semiconductors, exhibits both the *p*- and *n*-type conduction depending on the concentration of tin [4] and has an energy band gap of about 1.3 eV [5], between those of Si and GaAs. Normally, SnS has orthorhombic structure composing double layers of tightly bound Sn-S atoms with the bonding between layers extremely weak due to Van der Vaals forces [6]. Additionally, it has the advantage of its constituent elements being abundant in nature and not posing any health and environmental hazards. Therefore, SnS can be potentially used as a solar absorber in a thin film solar cell and near-infrared detector [7, 8], as photovoltaic materials [9] and as a holographic recording medium [10]. Therefore, Single crystalline SnS nanosheets reported in this paper are expected to offer enhanced properties. Therefore, it is important to investigate practical synthesis routes for novel SnS nanostructures, preferentially in single crystalline.

Tin sulfides show a variety of phases, such as SnS, Sn_2S_3, Sn_3S_4 and SnS_2, due to the versatile coordinating characteristics of tin and sulfur [11]. Normally, crystalline tin sulfides have been prepared by a varity of methods, such as direct vapor transport method [12], stoichiometric composition technique [13], physical vapor transport method [14] and Bridgman-Stockbarger technique [15]. In recent years, thin films of SnS have been investigated widely due to their applications in photovoltaic and photoelectrochemical (PEC) solar cells. SnS thin films have been prepared by spray pyrolytic deposition [16], eletrochemical depostion [17, 18], chemical vapor deposition [19, 20] and chemical bath deposition [21]. To our knowledge, preparation of novel sheet-like SnS nanostructures has not been reported. Qian *et al.* has reported solvothermal synthesis of SnS layered nanocrystallines and micrometer crystal belts using benzene and ethylenediamine as the solvent, respectively [22, 23]. In this paper, we have presented single crystalline SnS nanosheets prepared by a thioglyeolic acid (TGA) assisted hydrothermal method, which proves milder, simpler, more practical, and more environmentally friendly

*Author to whom all correspondence should be addressed.

than the solvothermal method. The synthesis route reported here offers great opportunity for scale-up preparation of SnS nanostructures.

2. Experimental details

All the reagents were of analytical grade without further purification. 0.001 mol of $SnCl_2 \cdot H_2O$ powder, 50 μL of thioglyeolic acid (TGA) and 100 ml of Na_2S aqueous solution with a concentration of 0.1 M were mixed slowly under stirring. After 10 min stirring, the final aqueous solution was transferred into a Teflon-lined autoclave of 150 ml capacity. The autoclave was maintained at 200°C for 48 h, and then cooled to room temperature naturally. The mixture turned black due to the formation of the SnS precipitates. The product was centrifugalized, washed with alcohol and deionized water for 3 times to remove the ions possibly remaining in the final product and finally dried at 60°C for 30 min in air.

An X-ray diffraction (XRD) pattern was obtained on a Rigaku D/max-ga X-ray diffractometer with graphite monochromatized CuKa radiation ($\lambda = 1.54178$ Å). Transmission electron microscopy (TEM) observation was performed on a Philips CM200 high-resolution transmission electron microscope (HRTEM) with an accelerating voltage of 200 kV.

3. Results and discussion

The XRD pattern of the as-prepared product is shown in Fig. 1. All the peaks of Fig. 1 can be indexed to the orthorhombic structure with lattice constants $a = 4.33$, $b = 11.19$, $c = 3.98$ Å, which are very consistent with the values in the standard card of SnS phase (JCPDS No. 39-0354). The strong and sharp diffraction peaks of Fig. 1 suggest that the SnS nanosheets are well crystallized. In addition, the XRD pattern of Fig. 1 is distinctive for the relative intensites of its sharp peaks greatly deviate from those of the standard card (JCPDS No. 39-0354). The great deviation resulted from highly anisotropic growth of the SnS crystals. The relative intensities of all sharp XRD peaks

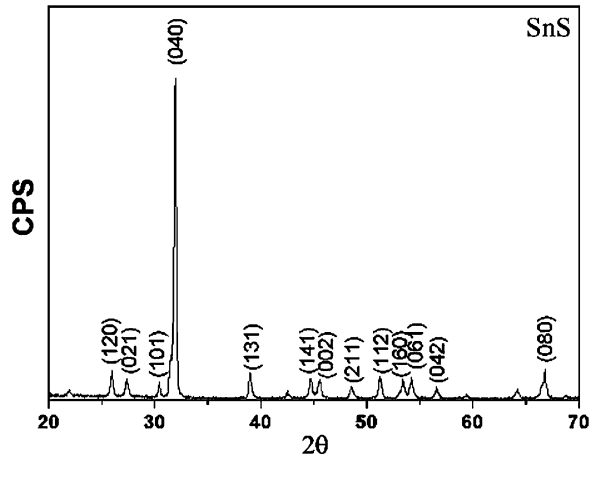

Figure 1 XRD pattern of the SnS nanosheets prepared by the TGA-assisted hydrothermal method.

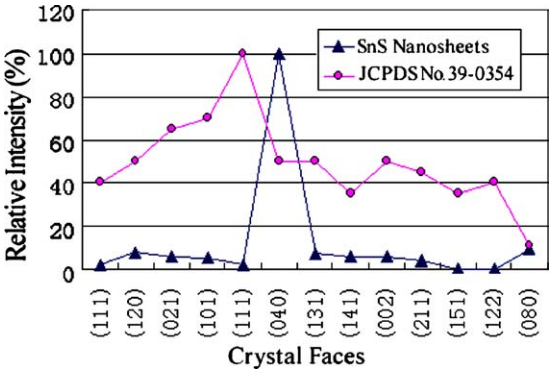

Figure 2 The relative intensities of sharp XRD peaks of the SnS nanosheets and the values in standard card (JCPDS No. 39-0354).

of the SnS nanosheets and the standard card (JCPDS No. 39-0354) are shown in Fig. 2. Fig. 2 illustrates that all the relative intensities of the SnS nanosheets is much smaller than those of the standard card except for those of (040) and (080) faces. It can be concluded that the SnS nanosheets might have a preferential [010] growth direction. More interestingly, the peak of (111) crystal face, the strongest peak in the standard card, dramatically decreases to almost zero. We conclude that the growth of the SnS nanosheets along [111] direction was strongly held back. Consequently, it can be concluded that the surface of the nanosheets may be (111) crystal face.

Typical TEM images and selected area electron diffraction (SAED) pattern of the SnS nanosheets are shown in Fig. 3, which reveal that the SnS crystals are of a novel sheet-like nanomorphology with several micrometers in width. Fringe contrast is observed in the TEM images of the SnS nanosheets and it is clearly shown in the amplified TEM image of a single nanosheet as illustrated in Fig. 3b. The formation of the fringe contrast of the TEM images was due to minute bending of the SnS nanosheets resulted from stress. Further structure characterization by SAED shows that the SnS nanosheets are single crystalline in nature, and the typical SAED pattern is presented in Fig. 3d. As discussed above, the SAED pattern of Fig. 3d can be indexed as the orthorhombic structure. According to their orthorhombic structure of the SnS nanosheets and SAED pattern of Fig. 3d, it can be concluded that the zone axis direction of the SAED pattern is [111] direction. In other words, the surface of the SnS nanosheet is (111) crystal face, being very consistent with the conclusion drawn from Fig. 2.

The formation mechanism of the SnS nanosheets is an interesting subject. Jinwoo Cheon *et al.* reported that the final shape of the obtained crystals is determined by competitive growth along different crystalline directions [24]. As discussed above, the SnS nanosheets were formed because the growth of the SnS nuclei along [111] direction was greatly held back and the growth along directions perpendicular to [111] direction was prefered. Based on above discussion, a sketch of growth mechanism of the SnS nanosheets under the TGA-assisted hydrothermal condition was put forward and is shown in Fig. 4.

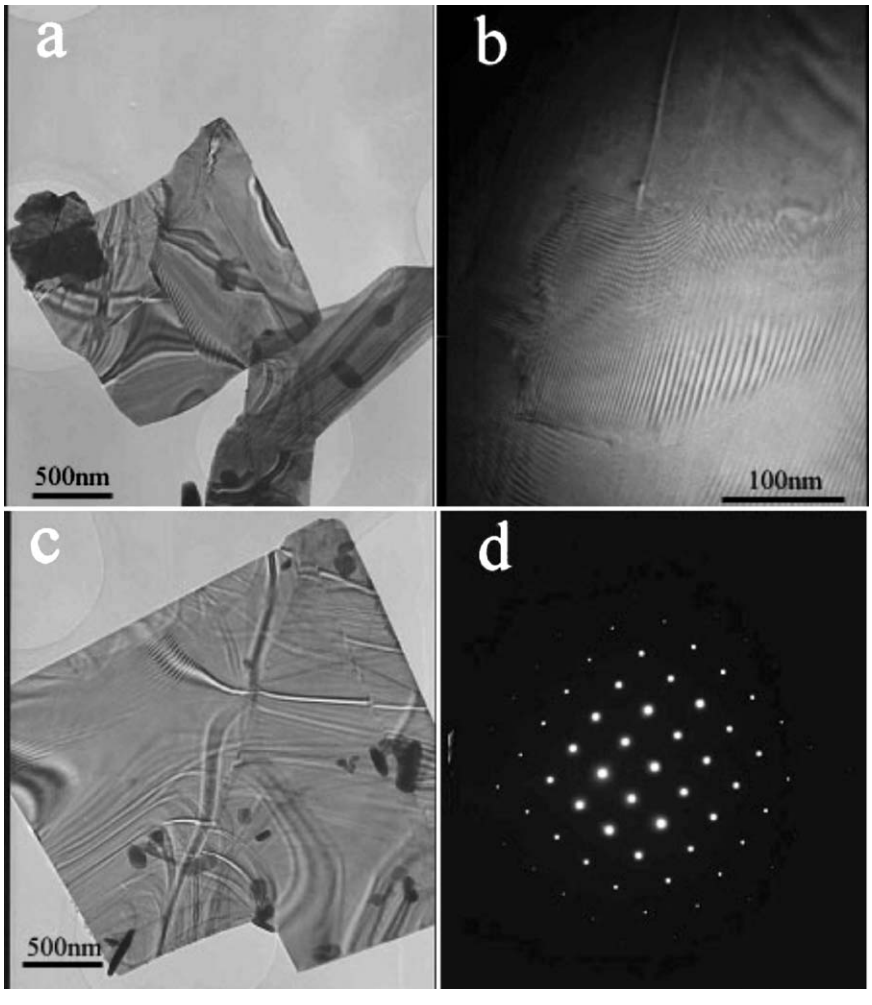

Figure 3 TEM images and SAED pattern of the SnS nanosheet: (a) TEM image of several SnS nanosheets, (b) amplified TEM image of a single nanosheet, (c) TEM image of a single nanosheet, and (d) SAED pattern of the nanosheet.

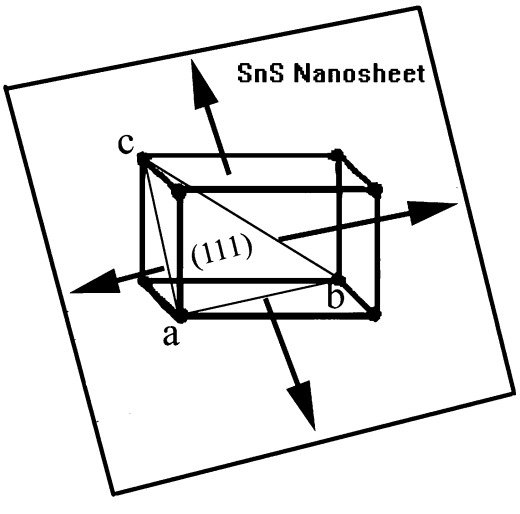

Figure 4 Schematic illustration of the growth mechanism of the SnS nanosheets.

In our synthetic system, the formation of the SnS nanosheets implied the nucleation and growth of the SnS crystals were well controlled. We believe that the TGA, which was used as a stability agent preventing nanocrystals from aggregating [25, 26], played a critical role on controlling the nucleation and growth of the SnS nanosheets. The detailed mechanism can be expressed as follows:

$$SnCl_2 + Na_2S \Rightarrow SnS \downarrow + 2NaCl \quad (1)$$

$$mSnS + kHSCH_2COOH + kSn^{2+} \Rightarrow (SnS)_m \times (SnSCH_2COOH)_k^{k+} + kH^+ \quad (2)$$

$$(SnS)_m(SnSCH_2COOH)_k^{k+} \Rightarrow (SnS)_m(Sn^{2+})_k + kSCH_2COOH^- \quad (3)$$

$$(SnS)_m(Sn^{2+})_k + kS^{2-} \Rightarrow (m+k)SnS \quad (4)$$

Prior to the hydrothermal process, SnS nuclei were formed via reactions (1). Compared with the conventional hydrothermal process, in the TGA-assisted hydrothermal process the marked difference is the formation of $(SnS)_m(SnSCH_2COOH)_k^{k+}$ complex clusters in the solution via reaction (2). Reaction (3) represents the dissociation of SCH_2COOH^- from the SnS complex clusters. Furthermore, We believe that the dissociation of SCH_2COOH^- occured in a local region of the complexed SnS cluster, where there were Sn^{2+} exposed to the S^{2-} existing in the solution. Therefore, during the TGA-assisted hydrothermal process, the formation of the SnS nanosheets proceeded along specific directions.

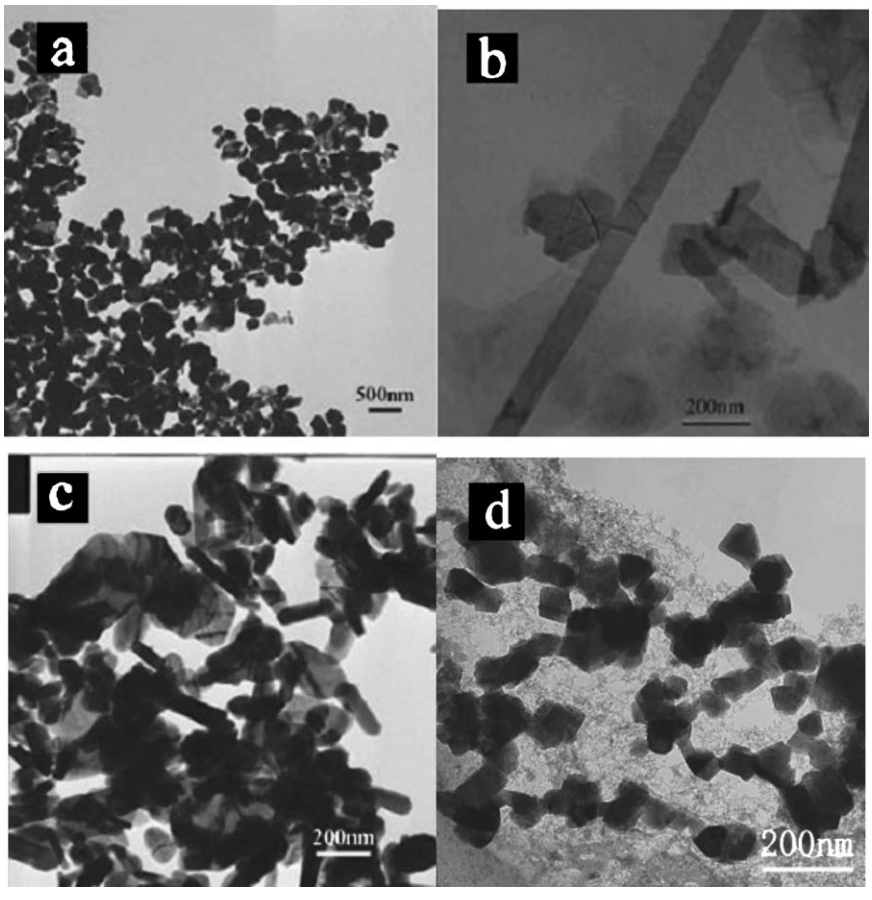

Figure 5 TEM images of the products synthesized by changing one of the synthesis factors (TGA, Sn/S ratio and hydrothermal temperature) while keeping other conditions unchanged: (a) synthesized by non-TGA-assisted hydrothermal process, (b) synthesized by using the Sn-S ratio of 1:4, (c) synthesized by using the Sn-S ratio of 1:2, and (d) hydrothermally synthesized at 120°C.

In the TGA-assisted hydrothermal process, TGA, Sn/S ratio and hydrothermal temperature make critical roles in the formation of the SnS nanosheets. To verify these points, non-TGA-assisted hydrothermal process was employed to synthesize SnS, while keeping other conditions unchanged. In this case, only irregular SnS nanoparticles was obtained as shown in Fig. 5a. Different Sn-S ratios such as 1:4 and 1:2 were used while keeping other conditions unchanged. Consequently, SnS_2 nanobelts and particles were obtained, respectively. Their TEM images are shown in Fig. 5b and c, respectively. When the hydrothermal temperature decreased to 120°C, irregular particles of SnS and SnO were obtained as shown in Fig. 5d. Therefore, TGA, Sn-S ratio and hydrothermal temperature are three key factors for the hydrothermal synthesis of the SnS nanosheets.

4. Conclusion

In summary, novle single-crystalline SnS nanosheets have been successfully prepared by a TGA-assisted hydrothermal method, with the advantages of simplicity, cost-effectiveness and reduced environmental impact. The growth mechanism and critical factors for the TGA-assisted hydrothermal synthesis of the SnS nanosheets have been discussed. Furthermore, it is reasonable to believe that the TGA-assisted hydrothermal process offers great opportunities for scale-up preparation of other chalcogenide nanostructures.

Acknowledgements

The authors would like to appreciate the financial supports of 863 project (No. 2001AA513023), the Natural Science Foundation of China (No. 60225010) and the Zhejiang Provincial Natural Science Foundation of China (No. 601092).

References

1. X. DUAN, Y. HUANG, R. AGARWAL and C. M. LIEBER, *Nature* **421** (2003) 241.
2. M. S. FUHRER, J. NYGARD, L. SHIH, M. FORERO, YOON YOUNG-GUI, M. S. C. MAZZONI and CHOI HYOUNG JOON, *Science* **288** (2000) 494.
3. Z. F. REN, Z. P. HUANG, J. W. XU, J. H. WANG, P. BUSH, M. P. SIEGAL and P. N. PROVENCIO, *ibid.* **282** (1998) 1105.
4. M. RISTOV, G. SINADINOVSKI, I. GROZDANOV and M. MITRESKI, *Thin Solid Films* **173** (1989) 53.
5. R. H. BUBE, "Photoconductivity of Solids" (Wiley, New York, 1960).
6. A. GHAZALI, Z. ZAINAL, M. Z. HUSSEIN and A. KASSIM, *Sol. Enger. Mater. Sol. Cells* **55** (1998) 237.
7. P. PRAMANIK, P. K. BASU and S. BISWAS, *Thin Solid Films* **150** (1987) 269.
8. N. K. REDDY and K. T. R. REDDY, *ibid.* **325** (1998) 4.
9. J. P. SINGH and R. K. BEDI, *ibid.* **199** (1991) 9.
10. M. RADOT, *Rev. Phys. Appl.* **18** (1977) 345.
11. T. JIANG and G. A. OZIN, *J. Mater. Chem.* **8** (1998) 1099.
12. S. K. ARORA, D. H. PATEL and M. K. AGARWAL, *J. Cryst. Growth* **131** (1993) 268.
13. E. P. TRIFONOVA, I. Y. YANCHEV, V. B. STOYANOVA, S. MANDALIDIS, K. KAMBAS and A. N. ANAGONOSTOPOULOS, *Mater. Res. Bull.* **31** (1996) 919.

14. J. GEORGE, C. K. VALSALA KUMARI and K. S. JOSEPH, *J. Appl. Phys.* **54** (1983) 5347.
15. M. J. POWEL, *J. Phys. C: Solid State Phys.* **10** (1977) 2967.
16. B. THANGARAJU and P. KALIANNAN, *J. Phys. D: Appl. Phys.* **33** (2000) 1054.
17. M. ICHIMURA, K. TAKEUCHI, Y. ONO and E. ARAI, *Thin Solid Films* **361/362** (2000) 98.
18. B. SUBRAMANIAN, C. SANJEEVIRAJA and M. JAYACHANDRAN, *Mater. Chem. Phys.* **71** (2001) 40.
19. A. ORTIZ, J. C. ALONSO, M. GARCIA and J. TORIZ, *Semicond. Sci Technol.* **11** (1996) 243.
20. L. S. PRICE, I. P. PARKIN, M. N. FIELD, A. M. E. HARDY, R. J. H. CLARK, T. G. HIBBERT and K. C. MOLLOY, *J. Mater. Chem.* **10** (2000) 527.
21. A. TANUŠEVSKI, *Semicond. Sci. Technol.* **18** (2003) 501.
22. Q. LI, Y. DING, H. WU, X. LIU and Y. QIAN, *Mater. Res. Bull.* **37** (2002) 925.
23. C. AN, K. TANG, G. SHEN, C. WANG, Q. YANG, B. HAI and Y. QIAN, *J. Cryst. Growth* **244** (2002) 333.
24. S. M. LEE, S. N. CHO and J. W. CHEON, *Adv. Mater.* **15** (2003) 441.
25. M. GAO, S. KIRSTEIN and H. MOHWALD, *J. Phys. Chem. B* **102** (1998) 8360.
26. D. HAYS, O. MIEIE, M. NENADOVIE, V. SWAYAMBUNATHAN and D. MEISEL, *ibid.* **93** (1989) 4603.

Received 31 August
and accepted 7 October 2004